Supporting Information for "Effect of a Cationic Surfactant on Droplet Wetting on Superhydrophobic Surfaces"

Ahmed Aldhaleai[1] and Peichun Amy Tsai[1,†]

[1]*Department of Mechanical Engineering,*
University of Alberta, Edmonton, Alberta, Canada T6G 1H9

Number of pages: 17
Number of figures: 13
Number of schemes: 0
Number of tables: 0

Abstract

In this supplementary material, we first include the detailed experimental data of contact angle using a flat hydrophobic substrate and two types of superhydrophobic (SH) surfaces studied. Second, we report the fitting method and parameters of the surfactant adsorption isotherms model. Third, we also show the free energy derivation for predicting the experimentally observed wetting states. Finally, we include the detailed derivation of the metastability criterion for a Cassie–Baxter state.

[†] peichun.amy.tsai@ualberta.ca

1. CONTACT ANGLE DATA OF SURFACTANT-LADEN DROPLETS ON FLAT HYDROPHOBIC AND SUPERHYDROPHOBIC SURFACES

Here we report the detailed contact angle measurements of a DDAB-laden droplet on both flat PDMS and two types of SH surfaces, S1 (r = 2.31, ϕ = 0.34) and S2 (r = 1.33, ϕ = 0.08), for nine different DDAB concentrations, and for ten droplets on each surface. On the one hand, for the higher-r SH S1, droplets were in a CB state for $C_S \leq 0.25$ CMC and in a W state for $C_S \geq 0.5$ CMC. On the other, both a CB and W state could appear for droplets on the lower-r SH S2 for $C_S \leq 0.75$ CMC, while all the surfactant-laden droplets were in a W state for C_S = 1 CMC.

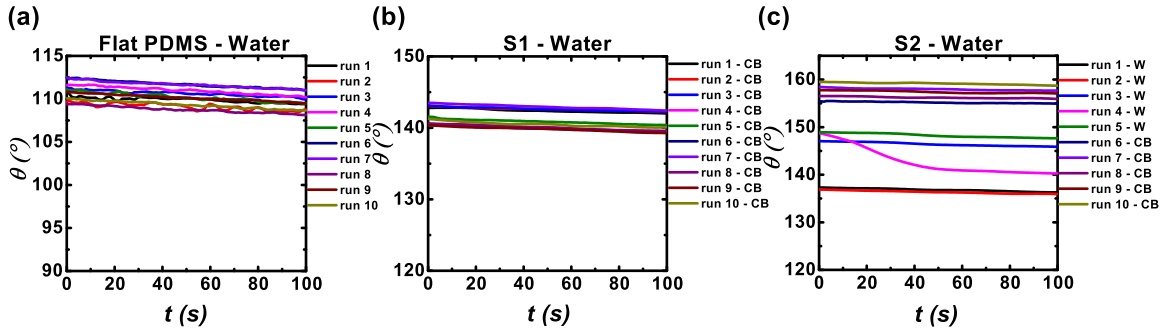

FIG. S1 Contact angle measurements for a pure-water droplet on (a) Flat PDMS, (b) SH S1 (r = 2.31, ϕ = 0.34), and (c) SH S2 (r = 1.33, ϕ = 0.08) surfaces during a period of 100s right after the droplet deposition.

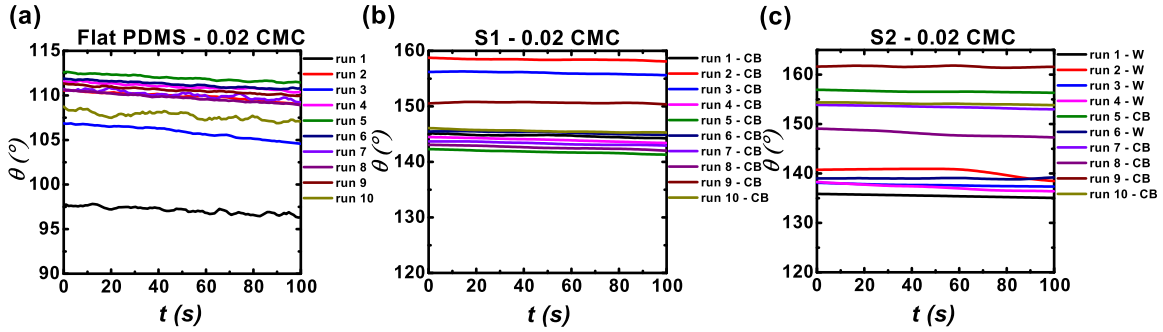

FIG. S2 Contact angle measurements for 0.02 CMC-DDAB droplet on (a) Flat PDMS, (b) SH S1 (r = 2.31, ϕ = 0.34), and (c) SH S2 (r = 1.33, ϕ = 0.08) surfaces during a period of 100s right after the droplet deposition.

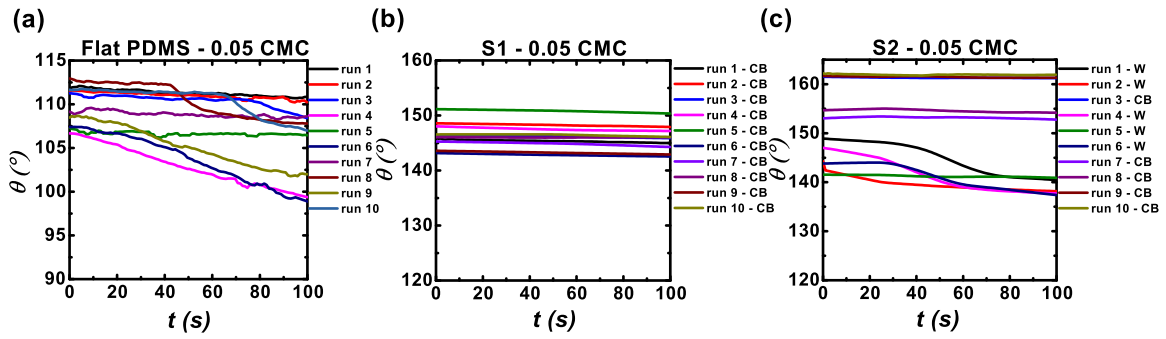

FIG. S3 Contact angle measurements for 0.05 CMC-DDAB droplet on (a) Flat PDMS, (b) SH S1 ($r = 2.31$, $\phi = 0.34$), and (c) SH S2 ($r = 1.33$, $\phi = 0.08$) surfaces during a period of 100s right after the droplet deposition.

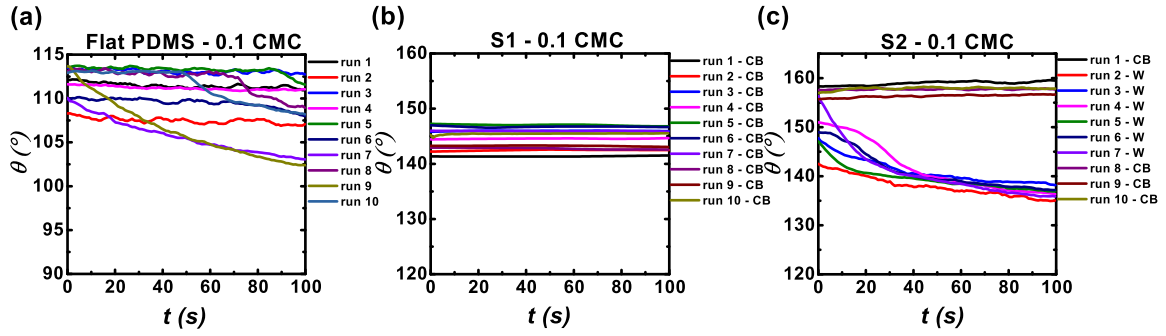

FIG. S4 Contact angle measurements for 0.1 CMC-DDAB droplet on (a) Flat PDMS, (b) SH S1 ($r = 2.31$, $\phi = 0.34$), and (c) SH S2 ($r = 1.33$, $\phi = 0.08$) surfaces during a period of 100s right after the droplet deposition.

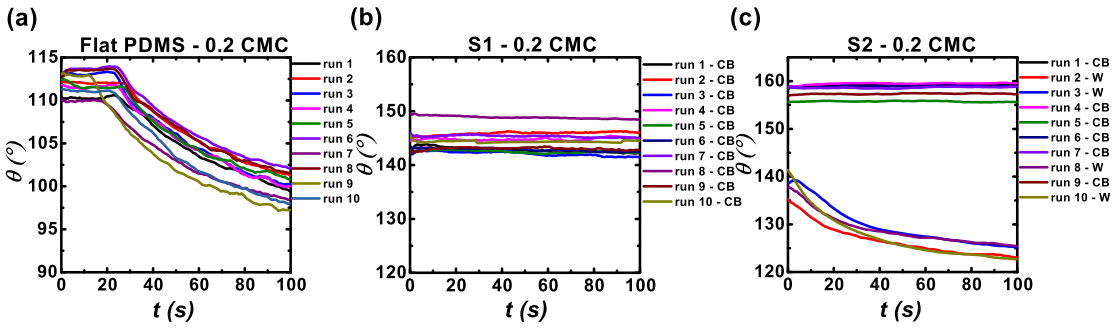

FIG. S5 Contact angle measurements for 0.2 CMC-DDAB droplet on (a) Flat PDMS, (b) SH S1 ($r = 2.31$, $\phi = 0.34$), and (c) SH S2 ($r = 1.33$, $\phi = 0.08$) surfaces during a period of 100s right after the droplet deposition.

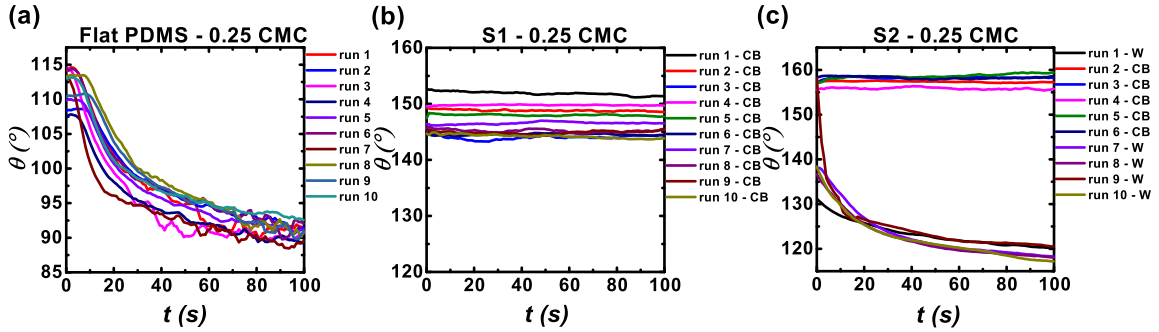

FIG. S6 Contact angle measurements for 0.25 CMC-DDAB droplet on (a) Flat PDMS, (b) SH S1 ($r = 2.31$, $\phi = 0.34$), and (c) SH S2 ($r = 1.33$, $\phi = 0.08$) surfaces during a period of 100s right after the droplet deposition.

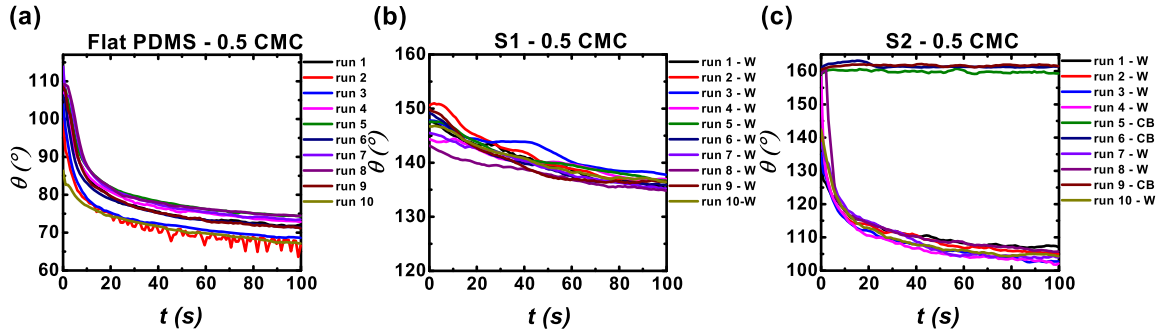

FIG. S7 Contact angle measurements for 0.5 CMC-DDAB droplet on (a) Flat PDMS, (b) SH S1 ($r = 2.31$, $\phi = 0.34$), and (c) SH S2 ($r = 1.33$, $\phi = 0.08$) surfaces during a period of 100s right after the droplet deposition.

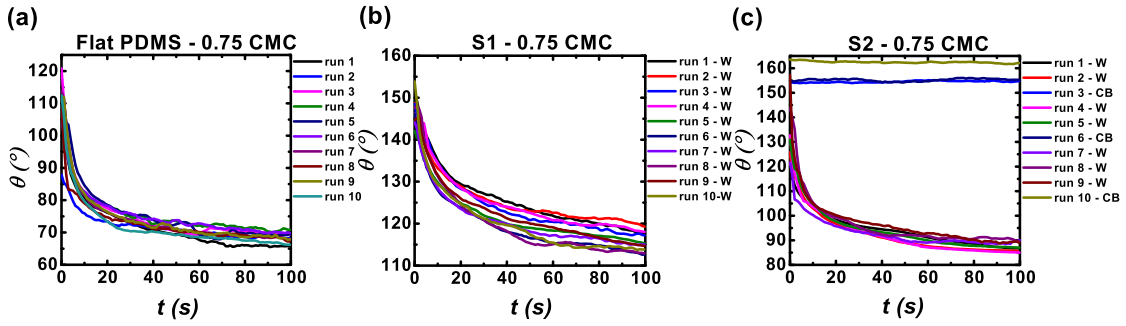

FIG. S8 Contact angle measurements for 0.75 CMC-DDAB droplet on (a) Flat PDMS, (b) SH S1 ($r = 2.31$, $\phi = 0.34$), and (c) SH S2 ($r = 1.33$, $\phi = 0.08$) surfaces during a period of 100s right after the droplet deposition.

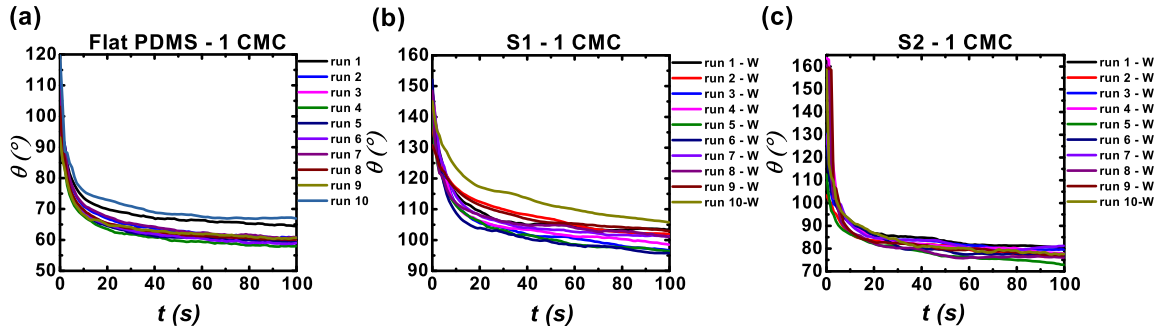

FIG. S9 Contact angle measurements for 1 CMC-DDAB droplet on (a) Flat PDMS, (b) SH S1 ($r = 2.31$, $\phi = 0.34$), and (c) SH S2 ($r = 1.33$, $\phi = 0.08$) surfaces during a period of 100s right after the droplet deposition.

2. FITTING OF WETTING DATA FROM FLAT PDMS SURFACES TO DETERMINE LIQUID-VAPOR AND SOLID-LIQUID ADSORPTION COEFFICIENTS

To account for the adsorption fitting parameters for LV and SL interfaces, we first use the Zhu–Gu adsorption isotherm [1] at the LV interface. We extracted LV interfacial tension, $\gamma_{\mathrm{LV}}(C_{\mathrm{S}})$, for DDAB aqueous solution droplets at the studied concentrations from two studies by Biswal-Paria [2, 3] and subsequently used the averaged values for our analysis. Fig.S10 shows a gradual decrease in the LV interfacial tension with increasing DDAB concentration. The best fit of eq. (3) in the main text to the data is also shown in Fig.S10. The fit was obtained using MATLAB's curve fitting 'cftool'. To solve the singularity at $\ln(C_{\mathrm{S}}) \to -\infty$, a pure water interfacial tension (γ^0_{LV}) was used as a fitting parameter. The best fitting parameters obtained include: $\Gamma^{\infty}_{\mathrm{LV}} = 4.679 \times 10^{-6}\ mol/m^2$, $n_{\mathrm{LV}} = 1.235$, $K_{\mathrm{LV}} = 191.5$, and $\gamma^0_{\mathrm{LV}} = 72.2\ mJ/m^2$, with goodness of fit parameters, SSE (Sum Squared Error): 6.879×10^{-6}, $R^2 : 0.9652$, adjusted-$R^2 : 0.9512$, and RMSE (Root Mean Square Error):$1.173 \times 10^{-3} J/m^2$. The fitting parameter $\Gamma^{\infty}_{\mathrm{LV}}$ is the maximum surfactant concentration at the liquid–vapor interface, K_{LV} is the adsorption equilibrium constant, and n_{LV} is an empirical fitting parameter.

To account for the surfactant adsorption at the SL interface, we use the Zhu–Gu adsorption isotherm [1] and arrive at the form of Milne et al. [4] modified Young equation, eq. (4) in the main text, which quantifies the contact angle of a drop on a flat and homogeneous

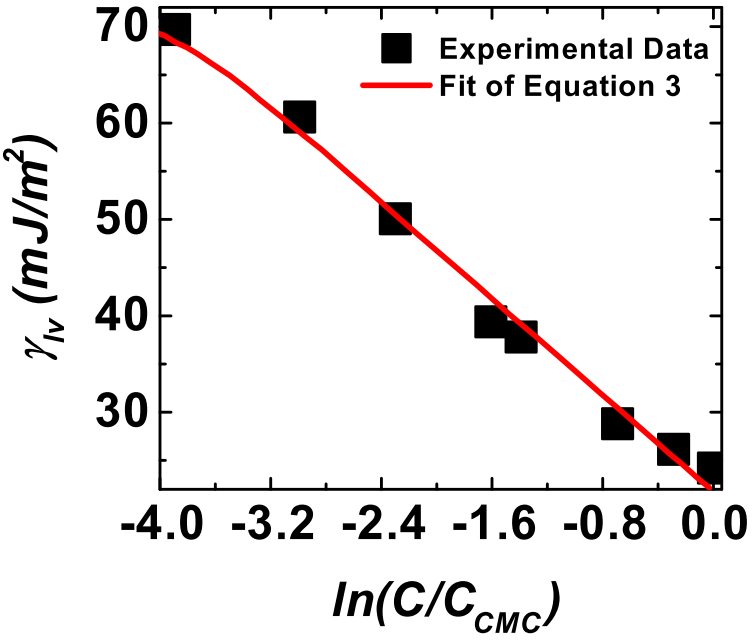

FIG. S10 Liquid-vapor (LV) interfacial tension vs. DDAB concentration in natural logarithmic scale (C/C_{CMC}). The experimental data (■) is the average LV interfacial tension from two studies [2, 3]. The line is the best fit of eq. (3) in the main text to the experimental data. The fitting parameters obtained include: $\Gamma^{\infty}_{\mathrm{LV}} = 4.679 \times 10^{-6}$ mol/m^2, $n_{\mathrm{LV}} = 1.235$, $K_{\mathrm{LV}} = 191.5$, and $\gamma^{0}_{\mathrm{LV}} = 72.2\ mJ/m^2$, with the goodness of fitting parameters, SSE (Sum Squared Error): 6.879×10^{-6} , $R^2 : 0.9652$, adjusted-$R^2 : 0.9512$, and RMSE (Root Mean Square Error): $1.173 \times 10^{-3} J/m^2$.

surface as a function of surfactant concentration, by assuming no surfactant adsorption at the SV interface. The average contact angles for the first 10 s and last 10 s of a 100 s recording period are shown in Fig. S11 and S12, respectively, along with the best fit of eq. (4) in the main text to our data. The fitting was done using the same way as for the LV adsorption parameters and using the previously found values of $\Gamma^{\infty}_{\mathrm{LV}}$, n_{LV}, K_{LV}, and γ^{0}_{LV}. The singularity at $\ln(C_{\mathrm{S}}) \to -\infty$ was solved by using the contact angle for pure water ($C_{\mathrm{S}} = 0$) as a fitting parameter. The best fitting parameters found for the first 10 s as in Fig.S11 were: $\Gamma^{\infty}_{\mathrm{SL}} = 2.979 \times 10^{-6} mol/m^2$, $n_{\mathrm{SL}} = 1.171$, $K_{\mathrm{SL}} = 114$, and $\theta^{0}_{\mathrm{Y}} = 110.84°$, with goodness of fit parameters, SSE: 1.803×10^{-3}, $R^2 : 0.9921$, adjusted-R^2: 0.989, and RMSE: 0.01899. The fitting parameters found for the last 10 s as in Fig. S12 were: $\Gamma^{\infty}_{\mathrm{SL}} = 3.819 \times 10^{-6} mol/m^2$, $n_{\mathrm{SL}} = 1.311$, $K_{\mathrm{SL}} = 188.1$, and $\theta^{0}_{\mathrm{Y}} = 109.43°$, with goodness of fit parameters, SSE: 5.343×10^{-3},

R^2 : 0.9916, adjusted-R^2 : 0.9882, and RMSE: 0.03269. The fitting parameter of Γ_{SL}^{∞} is the maximum surfactant concentration at the solid-liquid interface, K_{SL} is the adsorption equilibrium constant, and n_{SL} is an empirical fitting parameter. Based on the fitting parameters, both LV and SL adsorption process are in the same order of magnitude (10^{-6}) and together contribute to decrease θ_Y as C_S increases.

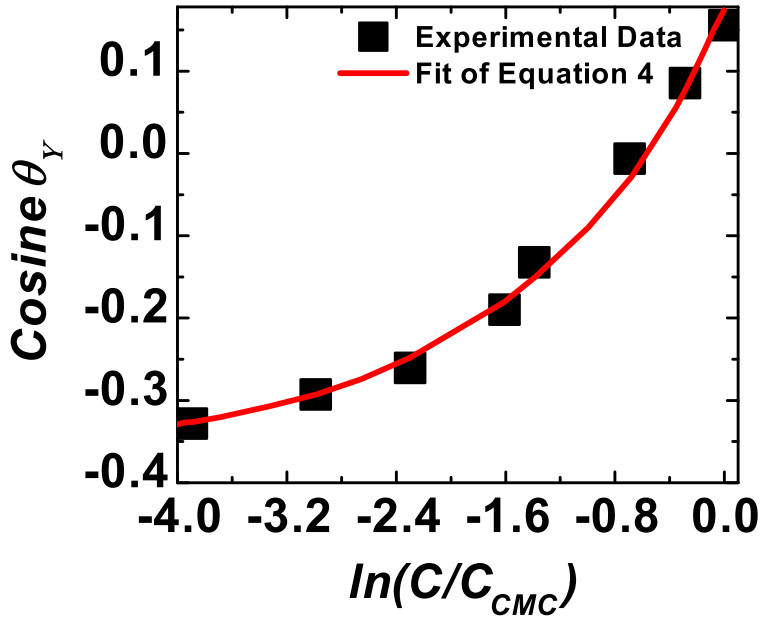

FIG. S11 Cosine of average contact angle on flat PDMS vs. DDAB concentration in natural logarithmic scale (C/C_{CMC}). The experimental contact angle (■) is the average of first 10 s of 100 s recording period. The line is the best fit of eq. (4) in the main text to the experimental data. The fitting parameters are: Γ_{SL}^{∞} = $2.979 \times 10^{-6} mol/m^2$, n_{SL} = 1.171, K_{SL} = 114, and θ_Y^0 = 110.84°, with goodness of fit parameters, SSE: 1.803×10^{-3}, R^2 : 0.9921, adjusted-R^2: 0.989, and RMSE: 0.01899.

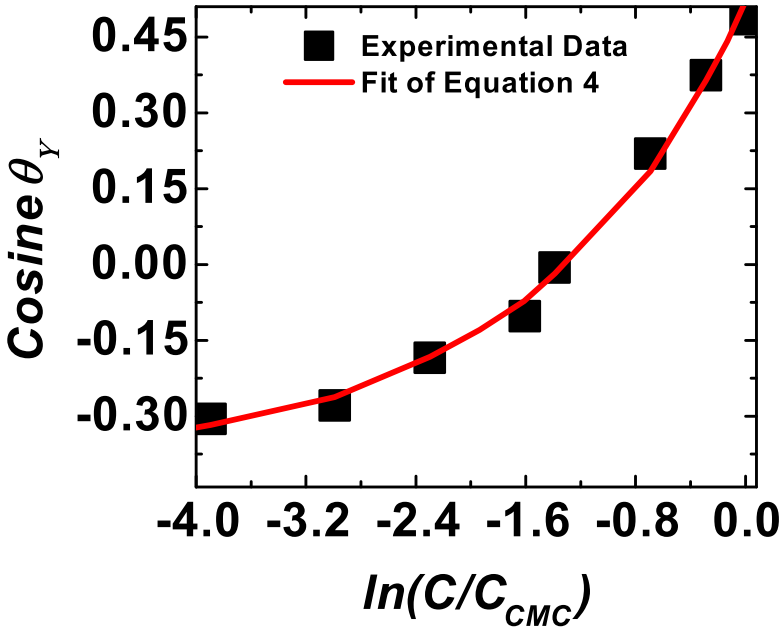

FIG. S12 Cosine of average contact angle on flat PDMS vs. DDAB concentration in natural logarithmic scale (C/C_{CMC}). The experimental contact angle (■) is the average of last 10 s of 100 s recording period. The line is the best fit of eq. (4) in the main text to the experimental data. The fitting parameters are: $\Gamma_{\mathrm{SL}}^{\infty} = 3.819 \times 10^{-6} mol/m^2$, $n_{\mathrm{SL}} = 1.311$, $K_{\mathrm{SL}} = 188.1$, and $\theta_{\mathrm{Y}}^{0} = 109.43°$, with goodness of fit parameters, SSE: 5.343×10^{-3}, $R^2 : 0.9916$, adjusted-$R^2 : 0.9882$, and RMSE: 0.03269.

3. FREE ENERGY DERIVATIONS FOR DIFFERENT WETTING STATES

In the derivation, we start from fundamental thermodynamic theories to derive the free energy and finally use this free energy to describe the effect of DDAB-surfactant concentration on a stable Cassie-Baxter and Wenzel wetting state. The free energy analysis of different wetting states of CB and Wenzel was first proposed by Johnson and Dettre [5], and other analyses have been performed for pure liquids on rough surfaces [6–10]. Here we closely follow the analytical approach of N. Shardt et al.[11] considering the effect of a surfactant on the free energies of different wetting states. Following Gibbsian composite-system thermodynamics [11–17], we consider a simplified geometry where the liquid phase has a spherical cap shape (curved), while the SL and SV interfaces are assumed to be flat. We also assume that there are no external forces, such as gravity or pinning/depinning forces at the three

phase contact line. According to this approach, the entire system is confined within a movable piston cylinder that interacts with a surrounding reservoir at constant pressure (P^R) and temperature (T^R). The reservoir can exchange energy and volume through the system boundary, but no mass exchange mass with the reservoir since the system is closed. Figure S13a shows the reference state assumed and in Fig. S13b a sessile drop with radius R and contact angle θ on a rigid solid. As shown in Fig. S13b, the assumed system is modeled as two bulk phases (or components). The first component consists of both liquid phase (e.g., water with surfactant) and the vapor phase, and the second component is the solid phase. Using the Gibbsian thermodynamics theory [12], the two phases are separated by a dividing surface that has the following thermodynamic quantities (internal energy, entropy, and moles). The equilibrium conditions of this closed system can be obtained by maximizing the entropy, S, so the differential of the entropy (dS) should equal to zero:

$$\mathrm{d}S^{\mathrm{L}} + \mathrm{d}S^{\mathrm{V}} + \mathrm{d}S^{\mathrm{LV}} + \mathrm{d}S^{\mathrm{S}} + \mathrm{d}S^{\mathrm{SL}} + \mathrm{d}S^{\mathrm{SV}} + \mathrm{d}S^{\mathrm{R}} = 0, \tag{S1}$$

where the superscripts L, V, LV, S, SL, SV, and R denote the liquid, vapor, liquid-vapor, solid, solid-liquid, solid-vapor, and reservoir phases, respectively.

Expressions in the differential form of the fundamental equation of thermodynamics of a bulk phase, a flat interface, or a curved interface is given by eqs. (S2), (S3), and (S4), which relate the changes in the internal energies, U due to the changes in the absolute temperature T, volume, V, pressure, P, the area, A, and chemical potential, μ:

$$\mathrm{d}U^{\mathrm{i}} = T^{\mathrm{i}}\mathrm{d}S^{\mathrm{i}} - P^{\mathrm{i}}\mathrm{d}V^{\mathrm{i}} + \sum_{\mathrm{j}=1}^{r} \mu_{\mathrm{j}}^{\mathrm{i}}\mathrm{d}N_{\mathrm{j}}^{\mathrm{i}}, \tag{S2}$$

$$\mathrm{d}U^{\mathrm{ab}} = T^{\mathrm{ab}}\mathrm{d}S^{\mathrm{ab}} + \gamma^{\mathrm{ab}}\mathrm{d}A^{\mathrm{ab}} + \sum_{\mathrm{j}=1}^{r} \mu_{\mathrm{j}}^{\mathrm{ab}}\mathrm{d}N_{\mathrm{j}}^{\mathrm{ab}}, \tag{S3}$$

$$\mathrm{d}U^{\mathrm{ab}} = T^{\mathrm{ab}}\mathrm{d}S^{\mathrm{ab}} + \gamma^{\mathrm{ab}}\mathrm{d}A^{\mathrm{ab}} + \sum_{\mathrm{j}=2}^{r} \mu_{\mathrm{j}}^{\mathrm{ab}}\mathrm{d}N_{\mathrm{j}}^{\mathrm{ab}}, \tag{S4}$$

where i denotes each phase, i.e., liquid, solid, or vapor, j is the phase component, either 1 or 2, N_{j} is the number of moles of component j, γ is the surface tension, and ab denotes each interface, i.e., SL, LV, or SV. To solve the free energy for this system, five constraints are imposed on the system, and we will discuss them below.

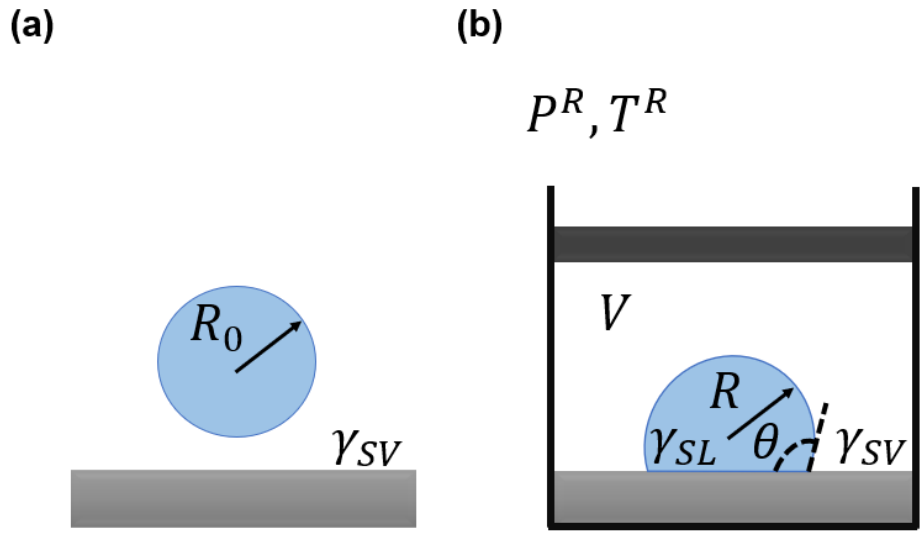

FIG. S13 (a) A Spherical drop without solid-liquid contact is assumed as the reference state. (b) Schematic of a piston-cylinder device in a reservoir containing a liquid drop in the shape of a spherical cap with contact angle θ and radius of curvature R on a rough, chemically homogeneous solid surface (with only component 1) in equilibrium with its vapor (V) and a solid surface (component 2).

Firstly, since the system is closed, there is no mass exchange between the reservoir and the system:

$$\mathrm{d}N_1^{\mathrm{R}} = 0 \qquad \mathrm{d}N_2^{\mathrm{R}} = 0. \tag{S5}$$

While component 1 can transfer between bulk phases and interfaces of the system,

$$\mathrm{d}N_1^{\mathrm{V}} + \mathrm{d}N_1^{\mathrm{L}} + \mathrm{d}N_1^{\mathrm{S}} + \mathrm{d}N_1^{\mathrm{LV}} + \mathrm{d}N_1^{\mathrm{SV}} + \mathrm{d}N_1^{\mathrm{SL}} + \mathrm{d}N_1^{\mathrm{R}} = 0. \tag{S6}$$

Secondly, both the reservoir and the system are isolated so that

$$\mathrm{d}U^{\mathrm{V}} = -\ \mathrm{d}U^{\mathrm{R}} - \mathrm{d}U^{\mathrm{S}} - \mathrm{d}U^{\mathrm{L}} - \mathrm{d}U^{\mathrm{SL}} - \mathrm{d}U^{\mathrm{SV}} - \mathrm{d}U^{\mathrm{LV}}. \tag{S7}$$

Thirdly, the system can exchange volume with the reservoir through the movable piston so

$$\mathrm{d}V^{\mathrm{R}} = -\ \mathrm{d}V^{\mathrm{V}} - \mathrm{d}V^{\mathrm{S}} - \mathrm{d}V^{\mathrm{L}}. \tag{S8}$$

Fourthly, the solid surface is assumed to be rigid (incompressible) means that no volume changes happen in the solid:

$$\mathrm{d}V^{\mathrm{S}} = 0. \tag{S9}$$

Finally, the solid surface is considered nonvolatile means that component 2 can only transfer between the solid phase and the SL and SV interfaces:

$$\mathrm{d}N_2^{\mathrm{S}} = -\,\mathrm{d}N_2^{\mathrm{SL}} - \mathrm{d}N_2^{\mathrm{SV}}. \tag{S10}$$

Based on the"Gibbs dividing surface" approach, the excess surface quantity (component 2) is assumed to be zero for the flat SL and SV interfaces, which means:

$$\mathrm{d}N_2^{\mathrm{SL}} = 0 \qquad \mathrm{d}N_2^{\mathrm{SV}} = 0 \quad \rightarrow \quad \mathrm{d}N_2^{\mathrm{S}} = 0. \tag{S11}$$

Also, it is worth mentioning here that for any increase or decrease in the SV interface area, there is an equivalent decrease or increase of the SL interfacial area: $A^{\mathrm{SV}} = -A^{\mathrm{SL}}$.

The volume of the spherical cap of the liquid drop, V^{L}, (shown in Fig. S13b) and areas for the LV and SL interfaces (A^{LV} and A^{SL}, respectively) can be written in terms of the radius of curvature, R, and the contact angle, θ [14, 16]:

$$V^{\mathrm{L}} = \int_0^{\theta} \pi R^3 \sin^3\varphi \; \mathrm{d}\varphi = \frac{\pi R^3}{3}\big(2 - \cos\theta(2 + \sin^2\theta)\big) = \frac{\pi R^3}{3}(2 - 3\cos\theta + \cos^3\theta), \tag{S12}$$

$$A^{\mathrm{LV}} = \int_0^{\theta} 2\pi R^2 \sin\varphi \; \mathrm{d}\varphi = 2\pi R^2(1 - \cos\theta), \tag{S13}$$

$$A^{\mathrm{SL}} = \pi R^2 \sin^2\theta. \tag{S14}$$

To obtain the equilibrium conditions for the defined system, we first take the differential forms of the volume and the interfacial areas, eqs. (S12)-(S14) (with respect to both R and θ). We subsequently substitute eqs. (S2) - (S4), the constraints (S5) - (S11), the derivatives of (S12) - (S14) into eq. (S1) and collect the similar terms, and get the following equation:

$$
\begin{aligned}
&\left(\frac{1}{T^{\mathrm{L}}}-\frac{1}{T^{\mathrm{V}}}\right)\mathrm{d}U^{\mathrm{L}}+\left(\frac{P^{\mathrm{R}}}{T^{\mathrm{R}}}-\frac{P^{\mathrm{V}}}{T^{\mathrm{V}}}\right)\mathrm{d}V^{\mathrm{R}}-\left(\frac{\mu_1^{\mathrm{L}}}{T^{\mathrm{L}}}-\frac{\mu_1^{\mathrm{V}}}{T^{\mathrm{V}}}\right)\mathrm{d}N_1^{\mathrm{L}}\\
&\quad+\left(\frac{1}{T^{\mathrm{S}}}-\frac{1}{T^{\mathrm{V}}}\right)\mathrm{d}U^{\mathrm{S}}+\left(\frac{1}{T^{\mathrm{LV}}}-\frac{1}{T^{\mathrm{V}}}\right)\mathrm{d}U^{\mathrm{LV}}\\
&\quad-\left(\frac{\mu_1^{\mathrm{LV}}}{T^{\mathrm{LV}}}-\frac{\mu_1^{\mathrm{V}}}{T^{\mathrm{V}}}\right)\mathrm{d}N_1^{\mathrm{LV}}+\left(\frac{1}{T^{\mathrm{SL}}}-\frac{1}{T^{\mathrm{V}}}\right)\mathrm{d}U^{\mathrm{SL}}\\
&\quad-\left(\frac{\mu_1^{\mathrm{SL}}}{T^{\mathrm{SL}}}-\frac{\mu_1^{\mathrm{V}}}{T^{\mathrm{V}}}\right)\mathrm{d}N_1^{\mathrm{SL}}+\left(\frac{1}{T^{\mathrm{SV}}}-\frac{1}{T^{\mathrm{V}}}\right)\mathrm{d}U^{\mathrm{SV}}\\
&\quad-\left(\frac{\mu_1^{\mathrm{SV}}}{T^{\mathrm{SV}}}-\frac{\mu_1^{\mathrm{V}}}{T^{\mathrm{V}}}\right)\mathrm{d}N_1^{\mathrm{SV}}+\left(\frac{1}{T^{\mathrm{R}}}-\frac{1}{T^{\mathrm{V}}}\right)\mathrm{d}U^{\mathrm{R}}\\
&\quad+\Big[\Big(\frac{P^{\mathrm{L}}}{T^{\mathrm{L}}}-\frac{P^{\mathrm{V}}}{T^{\mathrm{V}}}\Big)(2-\cos\theta(2+\sin^2\theta))\pi R^2\\
&\quad-\frac{\gamma^{\mathrm{LV}}}{T^{\mathrm{LV}}}(1-\cos\theta)4\pi R+\frac{(\gamma^{\mathrm{SV}}-\gamma^{\mathrm{SL}})}{T^{\mathrm{SL}}}(2\pi R\sin^2\theta)\Big]\,\mathrm{d}R\\
&\quad+\Big[\Big(\frac{P^{\mathrm{L}}}{T^{\mathrm{L}}}-\frac{P^{\mathrm{V}}}{T^{\mathrm{V}}}\Big)(\sin\theta(2+\sin^2\theta)-2\sin\theta\cos^2\theta)\frac{\pi R^3}{3}\\
&\quad-\frac{\gamma^{\mathrm{LV}}}{T^{\mathrm{LV}}}2\pi R^2\sin\theta+\frac{(\gamma^{\mathrm{SV}}-\gamma^{\mathrm{SL}})}{T^{\mathrm{SL}}}(2\pi R^2\sin\theta\cos\theta)\Big]\,\mathrm{d}\theta=0.
\end{aligned}
\tag{S15}
$$

For the above expression to be valid for any arbitrary displacement about equilibrium, the coefficients in front of each differential must be equal to zero. Setting all the coefficient of each independent variation to zero, yielding to the following equilibrium conditions:

$$T^{\mathrm{L}}=T^{\mathrm{LV}}=T^{\mathrm{S}}=T^{\mathrm{SL}}=T^{\mathrm{SV}}=T^{\mathrm{V}}=T^{\mathrm{R}}, \tag{S16}$$

$$\mu_1^{\mathrm{L}}=\mu_1^{\mathrm{LV}}=\mu_1^{\mathrm{SL}}=\mu_1^{\mathrm{SV}}=\mu_1^{\mathrm{V}}, \tag{S17}$$

$$P^{\mathrm{R}}=P^{\mathrm{V}}. \tag{S18}$$

In addition, the Laplace equation and Young equation can be obtained by setting the coefficients in front of dR and dθ to zero in eq. (S15) as follows:

$$P^{\mathrm{L}}-P^{\mathrm{V}}=\frac{2\gamma^{\mathrm{LV}}}{R}, \tag{S19}$$

$$\gamma^{\mathrm{SV}}-\gamma^{\mathrm{SL}}=\gamma^{\mathrm{LV}}\cos\theta. \tag{S20}$$

Given these equilibrium conditions, assuming that the pressure in the system is constant, and moving terms to the right-hand side, eq. (S15) is simplified to:

$$-(\gamma^{\mathrm{SV}}-\gamma^{\mathrm{SL}})A^{\mathrm{SL}}+\gamma^{\mathrm{LV}}A^{\mathrm{LV}}=0. \tag{S21}$$

Therefore, the total free energy of this system, E, is:

$$E = (\gamma^{SL} - \gamma^{SV})A^{SL} + \gamma^{LV}A^{LV}, \tag{S22}$$

which has the common form of the free energy as follows [12, 13, 15, 16]:

$$E = G^{V} + F^{L} + F^{S} + F^{SL} + F^{LV} + F^{SV} + P^{V}V^{L}, \tag{S23}$$

where G and F are Gibbs and Helmholtz free energies, respectively. As mentioned before, since the energy should be calculated with respect to a reference level, we choose the system of a spherical drop with no SL contact area as a reference point, and we assume that it is an equilibrium state. The total energy of this reference state, E_0, is given by:

$$E_0 = 4\pi R_0^2 \gamma^{LV}. \tag{S24}$$

Therefore, the change of the free energy of the current system with respect to the assumed reference point, $E - E_0$ is equal to:

$$E - E_0 = (\gamma^{SL} - \gamma^{SV})A^{SL} + \gamma^{LV}A^{LV} - 4\pi R_0^2 \gamma^{LV}, \tag{S25}$$

which has the same form as the free energy derived by Shardt et al. [11] for SDS surfactant drops on hydrophobic microstructures. If the current state of the system is also assumed in an equilibrium state, and by substituting the previous derived equilibrium condition, eq. (S20) and eq. (S13) - (S14) for the LV and SL areas, respectively, the final form of the free energy, $E - E_0$, is equal to:

$$E - E_0 = \pi R^2 \gamma^{LV}(2 - 3\cos\theta + \cos^3\theta) - 4\pi R_0^2 \gamma^{LV}, \tag{S26}$$

where E_0 is the reference free energy; defined as the free energy of a spherical drop with no SL contact, R is the spherical cap radius of curvature, R_0 is the initial radius of a spherical drop of 10 μl, and $\cos\theta = f\cos\theta_Y - f_1$. Here, f is the ratio of the SL surface area (pillar-top area) to the total (liquid-solid and liquid-gas) areas. f_1 is the ratio of the LV interfacial area to the total projected area beneath the drop. Finally, eq. (S26) can be used to predict the free energy difference related to the reference state for a CB, an intermediate, or a Wenzel state, depending on the parameter values of f and f_1.

A CB to Wenzel wetting transition may be modeled through two main processes [6, 14]. Initially, right after droplet deposition, a droplet wetting in the classical CB wetting state

has $f = \phi$ and $f_1 = 1-\phi$. In the first phase, the liquid penetrates the surface structure until it wets the bottom of the surface. We assume that the liquid wets the cylinders walls only, and the bottom surface is not wet, so the value of f increases from ϕ to $(\frac{\pi D^2}{4} + \pi DH)/(P^2)$ since the solid–liquid contact area increases and $f_1 = 1 - f$ does not change. In the second phase, liquid wets the bottom surface from the edges of pillars towards the center, as f continues to increase while $f_1 = r - f$ until the area below the drop is fully wetted. A full transition of the droplet to W occurs when $f = r$ and $f_1 = 0$, and hence $\cos\theta = r\cos\theta_{\mathrm{Y}}(C_{\mathrm{S}})$ as in the Wenzel equation [14, 18, 19].

4. DERIVATION OF THE METASTABILITY CRITERION FOR CASSIE-BAXTER STATE

To explain the stability and metastability of CB state, we use a similar approach to the proposed free energy analysis by Gong et al. for a pure water on a square-post microstructures [6]. They outline that there is an energy barrier between CB and W states based on the first derivative of the free energy barrier (i.e., $E_{max} - E_0$, where E_{max} is the maximum free energy state) with respect to the variable f as follows:

$$\left.\frac{\partial(E_{max} - E_{CB})}{\partial f}\right|_{f=\phi} > 0. \tag{S27}$$

Shardt et al. [6] used the same approach to analyze sodium dodecyl sulfate (SDS) surfactant-laden drops on hydrophobic microstructures. To apply eq. (S27), we first substitute the variable R in eq. (S26) by the corresponding value from the spherical cap volume approximation, i.e., eq. (S12). We subsequently replace the variable $\cos\theta$ by $\cos\theta = f\cos\theta_{\mathrm{Y}} - f_1$, where $f_1 = 1 - \phi$ as in the first process of CB-W transition. We obtained the energy barrier, $E_{max} - E_0$, by substituting all theses values into eq. (S26) and simplifying the equation:

$$E_{max} - E_0 = \pi^{1/3}(3V^{\mathrm{L}})^{2/3}\gamma^{\mathrm{LV}}\left\{2 - 3[f\cos\theta_{\mathrm{Y}} - (1-\phi)] + [f\cos\theta_{\mathrm{Y}} - (1-\phi)]^3\right\}^{1/3} - 4\pi R_0^2\gamma^{\mathrm{LV}}. \tag{S28}$$

The first partial derivative of eq. (S28) for the first process of CB-W transition with respect to f is:

$$\left.\frac{\partial(E_{max} - E_0)}{\partial f}\right|_{f=\phi} = \frac{\pi^{1/3}(3V^{\mathrm{L}})^{2/3}\gamma^{\mathrm{LV}}[3\cos\theta_{\mathrm{Y}}(f\cos\theta_{\mathrm{Y}} + \phi - 1)^2 - 3\cos\theta_{\mathrm{Y}}]}{3[(f\cos\theta_{\mathrm{Y}} + \phi - 1)^3 - 3(f\cos\theta_{\mathrm{Y}} + \phi - 1) + 2]^{2/3}}. \tag{S29}$$

Note that the common term in the nominator $\pi^{1/3}(V^{\mathrm{L}})^{2/3}\gamma^{\mathrm{LV}}$ and the denominator $3[(f\cos\theta_{\mathrm{Y}}+\phi-1)^3-3(f\cos\theta_{\mathrm{Y}}+\phi-1)+2]^{2/3}$ are always positive. To get the solution for eq. (S27) and based on the above observation, eq. (S29) is simplified to:

$$\cos\theta_{\mathrm{Y}}(\phi\cos\theta_{\mathrm{Y}}+\phi-1)^2-\cos\theta_{\mathrm{Y}}>0. \tag{S30}$$

The above equation can be simplified further to the following form:

$$\phi^2\cos^3\theta_{\mathrm{Y}}-2\phi(1-\phi)\cos^2\theta_{\mathrm{Y}}+(1-\phi)^2\cos\theta_{\mathrm{Y}}-\cos\theta_{\mathrm{Y}}>0. \tag{S31}$$

To solve for the ranges of $\cos\theta_{\mathrm{Y}}$ (or θ_Y) that fulfills the eq. (S31) criteria, we first set the left hand side of eq. (S31) = 0, which has three roots:

$$\cos\theta_{\mathrm{Y}}=-1,0,\frac{-\phi+2}{\phi}. \tag{S32}$$

Since the values of the packing fraction, ϕ, are restricted to the range between 0 and 1 ($0<\phi<1$), and the range of the cosine function is from -1 to 1, there is no possible solution for $(-\phi+2)/(\phi)$ because $(-\phi+2)/(\phi)$ is always greater than 1. Therefore, for the solution of eq. (S31) criteria to be valid for the presence of a metastable CB (i.e., with a presence of energy barrier), only two remaining roots are possible: $\cos\theta_{\mathrm{Y}}=-1$ and 0, which corresponds to $\theta_{\mathrm{Y}}=180^\circ$ and 90°, respectively. To fulfill the eq. (S31) criteria would require that the cosine function of the Young's equation should be $-1<\cos\theta_{\mathrm{Y}}<0$. In other words, the solution to eq. (S31) is $90^\circ<\theta_{\mathrm{Y}}<180^\circ$. Consequently, there is an energy barrier observed for both SH surfaces studied when $\theta_{\mathrm{Y}}>90^\circ$. In contrast, in the case of $\theta_{\mathrm{Y}}<90^\circ$, the first derivative of the free energy with respect to f will be less than 0 (as $\partial E/\partial f|_{f=\phi}<0$), and thus a stable W will always occur at any values of r and ϕ when $\theta_{\mathrm{Y}}<90^\circ$.

To locate the metastable regime, we used and calculated the critical point at the CB to Wenzel wetting transition, which is given by $\cos\theta_{\mathrm{Y}}^*=\frac{\phi-1}{r-\phi}$ (described in the main text) to locate the upper boundary, above which a CB state is more stable thermodynamically. For our two studied surfaces S1 ($\phi=0.34$ and $r=2.31$) and S2 ($\phi=0.08$ and $r=1.33$), the predicted critical Young angles are $\theta_{\mathrm{Y}}^*=109.6^\circ$ and $\theta_{\mathrm{Y}}^*=137.4^\circ$, respectively. Consequently, the metastable regime is located between 90° and θ_{Y}^* (see Fig. 6c in the main text). In this

$\theta_{\mathrm{Y}}(C_{\mathrm{S}})$-range, there is an energy barrier, and hence a CB state is metastable.

---

[1] Zhu, B.-Y.; Gu, T. General isotherm equation for adsorption of surfactants at solid/liquid interfaces. Part 1. Theoretical. *J. Chem. Soc., Faraday Trans. I* **1989**, *85*, 3813–3817.

[2] Biswal, N. R.; Paria, S. Wetting of PTFE and glass surfaces by aqueous solutions of cationic and anionic double-chain surfactants. *Ind. Eng. Chem. Res.* **2012**, *51*, 10172–10178.

[3] Biswal, N. R.; Paria, S. Interfacial and wetting behavior of natural–synthetic mixed surfactant systems. *RSC Advances* **2014**, *4*, 9182–9188.

[4] Milne, A.; Elliott, J.; Zabeti, P.; Zhou, J.; Amirfazli, A. Model and experimental studies for contact angles of surfactant solutions on rough and smooth hydrophobic surfaces. *Phys. Chem. Chem. Phys.* **2011**, *13*, 16208–16219.

[5] Johnson, R. E.; Dettre, R. H. Contact angle hysteresis: I. Study of an idealized rough surface. *Adv. Chem.* **1964**, *43*, 112–135.

[6] Gong, W.; Zu, Y.; Chen, S.; Yan, Y. Wetting transition energy curves for a droplet on a square-post patterned surface. *Sci. Bull.* **2017**, *62*, 136 – 142.

[7] Tsai, P.; Lammertink, R. G.; Wessling, M.; Lohse, D. Evaporation-triggered wetting transition for water droplets upon hydrophobic microstructures. *Phys. Rev. Lett.* **2010**, *104*, 2–3.

[8] Bussonnière, A.; Bigdeli, M. B.; Chueh, D.-Y.; Liu, Q.; Chen, P.; Tsai, P. A. Universal wetting transition of an evaporating water droplet on hydrophobic micro-and nano-structures. *Soft matter* **2017**, *13*, 978–984.

[9] Murakami, D.; Jinnai, H.; Takahara, A. Wetting transition from the Cassie–Baxter state to the Wenzel state on textured polymer surfaces. *Langmuir* **2014**, *30*, 2061–2067.

[10] Ren, W. Wetting transition on patterned surfaces: transition states and energy barriers. *Langmuir* **2014**, *30*, 2879–2885.

[11] Shardt, N.; Bigdeli, M. B.; Elliott, J. A.; Tsai, P. A. How Surfactants Affect Droplet Wetting on Hydrophobic Microstructures. *J. Phys. Chem. Lett.* **2019**, *10*, 7510–7515.

[12] Gibbs, J. W. On the equilibrium of heterogeneous substances. *Am. J. Sci.* **1878**, *16*, 441–458.

[13] Ward, C.; Levart, E. Conditions for stability of bubble nuclei in solid surfaces contacting a liquid-gas solution. *J. Appl. Phys.* **1984**, *56*, 491–500.

[14] Ishino, C.; Okumura, K.; Quéré, D. Wetting transitions on rough surfaces. *EPL* **2004**, *68*,

419–425.

[15] Elliott, J. A.; Voitcu, O. On the thermodynamic stability of liquid capillary bridges. *Can. J. Chem. Eng.* **2007**, *85*, 692–700.

[16] Eslami, F.; Elliott, J. A. Thermodynamic investigation of the barrier for heterogeneous nucleation on a fluid surface in comparison with a rigid surface. *J. Phys. Chem. B* **2011**, *115*, 10646–10653.

[17] Zargarzadeh, L.; Elliott, J. A. Comparative surface thermodynamic analysis of new fluid phase formation between a sphere and a flat plate. *Langmuir* **2013**, *29*, 3610–3627.

[18] Wenzel, R. N. Resistance of solid surfaces to wetting by water. *Ind. Eng. Chem.* **1936**, *28*, 988–994.

[19] Cassie, A.; Baxter, S. Wettability of porous surfaces. *J. Chem. Soc. Faraday Trans.* **1944**, *40*, 546–551.